AFRL-RX-WP-TP-2010-4051

MEASUREMENT OF γ' PRECIPITATES IN A NICKEL-BASED SUPERALLOY USING ENERGY-FILTERED TRANSMISSION ELECTRON MICROSCOPY COUPLED WITH AUTOMATED SEGMENTING TECHNIQUES (PREPRINT)

J.S.Tiley, G.B. Viswanathan, and A. Shiveley

Metals Branch
Metals, Ceramics & NDE Division

M. Tschopp

Mississippi State University

R. Srinivasan and H.L. Fraser

The Ohio State University

R. Banerjee

University of North Texas

JANUARY 2010

AIR FORCE RESEARCH LABORATORY
MATERIALS AND MANUFACTURING DIRECTORATE
WRIGHT-PATTERSON AIR FORCE BASE, OH 45433-7750
AIR FORCE MATERIEL COMMAND
UNITED STATES AIR FORCE

REPORT DOCUMENTATION PAGE

Form Approved
OMB No. 0704-0188

1. REPORT DATE *(DD-MM-YY)*	2. REPORT TYPE	3. DATES COVERED *(From - To)*
January 2010	Journal Article Preprint	01 January 2010 – 31 January 2010

4. TITLE AND SUBTITLE

MEASUREMENT OF γ' PRECIPITATES IN A NICKEL-BASED SUPERALLOY USING ENERGY-FILTERED TRANSMISSION ELECTRON MICROSCOPY COUPLED WITH AUTOMATED SEGMENTING TECHNIQUES (PREPRINT)

5a. CONTRACT NUMBER
In-house

5b. GRANT NUMBER

5c. PROGRAM ELEMENT NUMBER
62102F

6. AUTHOR(S)

J.S.Tiley, G.B. Viswanathan, and A. Shiveley (AFRL/RXLM)
M. Tschopp (Mississippi State University)
R. Srinivasan and H.L. Fraser (The Ohio State University)
R. Banerjee (University of North Texas)

5d. PROJECT NUMBER
4347

5e. TASK NUMBER
RG

5f. WORK UNIT NUMBER
M02R1000

7. PERFORMING ORGANIZATION NAME(S) AND ADDRESS(ES)

Metals Branch (AFRL/RXLM)
Metals, Ceramics & NDE Division Materials and Manufacturing Directorate
Wright-Patterson Air Force Base, OH 45433-7750
Air Force Materiel Command, United States Air Force

The Ohio State University
Center for the Accelerated Maturation of Materials
Department of Materials Science and Engineering
Columbus, OH 43210

Mississippi State University
Center for Advanced Vehicular Systems
Starkville, MS 39762

University of North Texas
Center for Advanced Research and Technology
Department of Materials Science and Engineering
Denton, TX 76203

8. PERFORMING ORGANIZATION REPORT NUMBER
AFRL-RX-WP-TP-2010-4051

9. SPONSORING/MONITORING AGENCY NAME(S) AND ADDRESS(ES)

Air Force Research Laboratory
Materials and Manufacturing Directorate
Wright-Patterson Air Force Base, OH 45433-7750
Air Force Materiel Command
United States Air Force

10. SPONSORING/MONITORING AGENCY ACRONYM(S)
AFRL/RXLMD

11. SPONSORING/MONITORING AGENCY REPORT NUMBER(S)
AFRL-RX-WP-TP-2010-4051

12. DISTRIBUTION/AVAILABILITY STATEMENT
Approved for public release; distribution unlimited.

13. SUPPLEMENTARY NOTES
Journal article submitted to Micron, to be published in 2010. PAO Case Number: 88ABW-2009-4246; Clearance Date: 01 Oct 2009. Paper contains color.

14. ABSTRACT

Precipitates of the ordered L12 γ' phase (dispersed in the face-centered cubic or FCC γ matrix) were imaged in Rene 88 DT, a commercial multicomponent Ni-based superalloy, using energy filtered transmission electron microscopy (EFTEM). Imaging was performed using the Cr, Co, Ni, Ti and Al elemental L-edges in the energy loss spectrum. Manual and automated segmentation procedures were utilized for identification of precipitate boundaries, measurement of precipitate sizes and overall area fractions. The automated region growing technique for precipitate identification in images was determined to accurately measure precipitate diameters. In addition, the region growing technique provided a repeatable method for optimizing segmentation techniques for varying EFTEM conditions.

15. SUBJECT TERMS
Rene 88 DT, energy filtered transmission electron microscopy (EFTEM)

16. SECURITY CLASSIFICATION OF:			17. LIMITATION OF ABSTRACT:	18. NUMBER OF PAGES	19a. NAME OF RESPONSIBLE PERSON (Monitor)
a. REPORT	b. ABSTRACT	c. THIS PAGE			Christopher F. Woodward
Unclassified	Unclassified	Unclassified	SAR	20	19b. TELEPHONE NUMBER *(Include Area Code)* N/A

Standard Form 298 (Rev. 8-98)
Prescribed by ANSI Std. Z39-18

Measurement of γ' Precipitates in a Nickel-based Superalloy using Energy-Filtered Transmission Electron Microscopy coupled with Automated Segmenting Techniques

J.S.Tiley[1], G.B. Viswanathan[1], A. Shiveley[1], M. Tschopp[1,4], R. Srinivasan[2], R. Banerjee[3], and H.L. Fraser[2]

1. Materials and Manufacturing Directorate, Air Force Research Laboratory, Dayton, OH 45433
2. Center for the Accelerated Maturation of Materials, Department of Materials Science and Engineering, The Ohio State University, Columbus OH 43210
3. Center for Advanced Research and Technology, Department of Materials Science and Engineering, University of North Texas, Denton TX 76203
4. Center for Advanced Vehicular Systems, Mississippi State University, Starkville MS 39762

Abstract

Precipitates of the ordered $L1_2$ γ' phase (dispersed in the face-centered cubic or FCC γ matrix) were imaged in Rene 88 DT, a commercial multicomponent Ni-based superalloy, using energy filtered transmission electron microscopy (EFTEM). Imaging was performed using the Cr, Co, Ni, Ti and Al elemental L-edges in the energy loss spectrum. Manual and automated segmentation procedures were utilized for identification of precipitate boundaries, measurement of precipitate sizes and overall area fractions. The automated region growing technique for precipitate identification in images was determined to accurately measure precipitate diameters. In addition, the region growing technique provided a repeatable method for optimizing segmentation techniques for varying EFTEM conditions.

1. Introduction

Ni-based superalloys are widely used as high temperature structural materials in aerospace propulsion systems. The typical microstructure in these materials consists of a dispersion of the ordered $L1_2$ γ' phase in an FCC γ matrix. It is widely known that several mechanical and physical properties are strongly dependent upon the morphology, size and volume fraction of the γ' precipitates [1-5]. These precipitates nucleate during the initial cooling from a supersolvus annealing temperature (solvus ~ 1124º C for Rene 88 DT), and the effect of cooling rate and subsequent aging treatments on the nucleation, growth and morphologies of these precipitates has been well documented [6-11]. Thus, developing techniques to accurately measure precipitate sizes and characterize precipitate morphologies is important. Several sample preparation and imaging techniques have been attempted in the past to study γ' precipitate attributes, with varying degrees of success. For example, the use of chemical etchants and electropolishing techniques to preferentially remove either the γ matrix material or the γ' precipitates can enhance the contrast of precipitate/matrix interfaces in SEM images [9]. While the larger secondary γ' precipitates (formed during the initial nucleation process while cooling from the supersolvus annealing temperature) can be imaged well through such procedures, such etching techniques may result in material loss at the boundaries; this can introduce significant errors in the subsequent measurement of sizes of smaller tertiary γ' precipitates, which normally form during a second nucleation burst during cooling and/or aging. Other techniques have focused on dissolution of the matrix followed by separation of the larger and smaller particles through settling and filtering [9,12,13]. However, such techniques may cause the tertiary γ' particles to

agglomerate with secondary γ' precipitates and carbides due to surface tension forces, thus complicating measurement and analysis.

In contrast, successful imaging of the tertiary γ' precipitates has been performed using Energy-Filtered TEM (EFTEM) [10,14,15]. The preferential segregation of elements between the γ and γ' phases generates image contrast in EFTEM. It has been reported that Al and Ti strongly segregate to the γ' phase, while Cr and Co segregate to the γ matrix [14, 15]. In contrast to earlier studies that have imaged γ' precipitates using several elemental edges depending upon the multicomponent nature of the alloys being investigated [15,16], this research utilizes the EFTEM technique to accurately determine precipitate sizes using multiple segmentation procedures.

Image analysis procedures that measure attributes of dispersed microstructural features typically involve the use of automated segmentation techniques and manual boundary region trace procedures. Various segmentation approaches have been used to measure the size of microstructural features based on grey scale intensity values [10,17-18]. For example, segmentation filters have been coupled with concurrent boundary trace methods to determine area fractions of equiaxed alpha in Ti-6Al-4V [17]. A similar manual trace method was used to measure the area fractions of secondary and tertiary γ' precipitates in Rene 88DT [10]. While the manual trace method is time consuming and influenced by selection of the boundary (which is difficult for precipitates with graded intensity contrast at the interface), many current automated approaches have trouble identifying microstructural features with diffuse interface regions in images with varying background intensity. Although the manual trace methods overcome this issue by using operator judgment, an element of subjectivity is introduced in the analysis. Clearly, techniques that can segment precipitates with diffuse interfaces in a repeatable, automated manner are highly desirable. This research focuses on determining the impact of using different elemental edges in EFTEM imaging, while comparing both manual and automated techniques for determining precipitate sizes.

1. Material and Methods

1.1 Processing and Imaging History

The commercial Ni- based superalloy Rene 88DT was selected for this study primarily because of its ability to produce γ' precipitates of various sizes (typically 5-300nm) depending on thermal processing. Effective imaging of these precipitates coupled with robust stereological methods to obtain size and distribution of γ' precipitates is vital to calibrate and validate the computational models that are currently being developed to predict the properties. A sample was cut for this research from a forged disc produced and tested under work supported by the Defense Advanced Research Projects Agency [19]. The bulk chemical composition of the Rene 88DT sample is given in Table I. The sample was solutionized at 1150° C to dissolve primary γ' and then water quenched and subsequently aged at 760° C for 25 hours to produce a fine dispersion of unimodal primary γ' precipitates. Segregation of alloying elements across the γ/γ' interface and compositions within the precipitate and matrix, as determined using 3-Dimensional Atom Probe (3DAP) Tomography [8], were used to determine the potential element edges for EFTEM imaging. TEM foils were prepared from the heat-treated sample according to the procedure described in reference [10]. Samples were analyzed in a Tecnai-F20 FEG/200 kV microscope.

Energy filtered transmission electron microscope (EFTEM) images were acquired using a Gatan image filter (GIF) with a slow scan YAG scintillator. The three-window method [15] was deployed using the power law function to correct the background using Digital Micrograph software. The experimental parameters for obtaining EFTEM images such as the types of ionization edges, operating slit widths for particular elements are listed in Table 2.

1.2 Image Analysis Procedures

Two types of image analysis procedures were employed to evaluate the precipitates. The first involved a manual trace method where the particle boundary was traced onto the image using Fovea Pro© [20] filters added to Photoshop© [21]. The traced particle size and its equivalent diameter were then determined based on the number of pixels, as described elsewhere [17]. For the second approach, image analysis was performed using an intensity-based technique developed with Labview© [22]. First, each particle and the adjacent surrounding matrix area was cropped from the image and analyzed as a separate image. This technique segmented each particle using user defined minimum and maximum threshold parameters. For instance, if a pixel intensity was greater than the minimum threshold parameter and less than the maximum threshold parameter, the pixel was assigned to the particle. Otherwise, the pixel was assigned to the matrix. A rectangular bounding box containing the segmented particle was then used for quantitative measures of particle size/diameter. Rules for connectivity were applied to refine the bounding box. Initially, the minimum and maximum threshold parameters for an eight bit image were set to 0 and 255, respectively. Three criteria were used to determine the number of pixels [23]:

1. In the Diagonal technique, the rectangular bounding box's height and width are calculated for each particle. This method tracks the diagonal distance (in pixels) between opposite corners of the bounding box.

2. In the Maximum Feret technique the maximum feret diameter (pixels) associated with the bounding box was calculated as below:

$$\text{Maximum Feret Diameter} = \sqrt{(F_{y2} - F_{y1})^2 + (F_{x2} - F_{x1})^2} \qquad (1)$$

   where F_{y1} and F_{y2} are the starting and ending feret diameters in the y direction, and F_{x1} and F_{x2} are the starting and ending feret diameters in the x direction.

3. In the Automated Area technique the number of pixels within the particle is counted.

The automated approaches were easily implemented with direct observation of the precipitate area during the procedure. That is, the real-time plots that showed how the particle pixel count changes with minimum threshold parameter allowed the user to manually identify when the precipitate boundary was crossed based on the slope of the plot.

2.3 Region Growing Technique

Several disadvantages associated with automated intensity routines were addressed through creating an automated region growing technique for segmenting the γ' precipitates [24]. First, to discourage non-spherical growth with the region growing technique, the addition process was modified to include a density-based weighting factor. Similar to the typical region growing algorithm, the intensity difference was calculated for each pixel neighboring the region. However, instead of adding the pixel with the closest intensity value, the intensity difference for each pixel was multiplied by a weighting factor function and the pixel with the lowest value was added. By multiplying this weighting factor by the intensity difference for each pixel, this places a higher (lower) probability of adding a pixel surrounded by a large (small) number of pixels belonging to the region. The weighting factor function is given by,

$$w(n) = \frac{e^c}{e^n} \qquad (2)$$

where *n* is the number of neighbors belonging to the region in a local neighborhood centered around each pixel and c is a constant that normalizes the weighting function such that the value of w(c) = 1.

Second, to eliminate the requirement of a user-specified threshold parameter and make this technique automated, the stopping feature of a typical region growing algorithm was modified. To accomplish this, the threshold parameter for the region growing algorithm was incrementally increased and a penalty function was calculated for each threshold parameter. In this study, the penalty function was chosen to be the difference between the mean intensity of the border just inside the region and the mean intensity of the border just outside the region (7 pixel thickness in both cases). The threshold parameter that maximized the penalty function was the critical threshold parameter that defined the optimum segmentation for the precipitate.

3. Results and Discussion

3.1 EFTEM imaging of γ' precipitates

Previous studies have shown that EFTEM imaging is a superior technique compared to CTEM and STEM methods for imaging fine γ' precipitates because of the elemental partitioning effect leading to better contrast in EFTEM images and its rapid acquisition capability. Recently, this method was effectively used in γ' coarsening studies by Tiley et.al [10] to determine size and morphological changes of these precipitates under varying heat treatment conditions. The authors in that study had primarily used the Cr-L ionization edge to image the precipitates. While Cr-L edge is still considered best suited for better contrast in the images, the use of ionization edges from other alloying elements (Ni,Ti,Al and Co) has not been explored to estimate the size of γ' precipitates. More recently, 3D atom probe (3DAP) tomography studies have shown that the γ / γ' interface is not abrupt but instead rather diffuse with a compositional gradient across the interface [25]. Hence, another aspect of this study is to see whether the subtle differences in the partitioning of different alloying elements seen in the 3D atom probe could impact the stereological measurements if EFTEM imaging of γ' precipitates was attempted with elements other than Cr.

Based on the 3DAP results shown in Figure 1, Cr shows the greatest segregation between the matrix and γ' precipitates while Mo shows very little partitioning [8]. Specifically, Cr, and Co segregate to the matrix material while Ti, Ni, and Al segregate to the precipitate. Figure 2 shows examples of the elemental maps obtained using the L-edges for Ti, Cr, Ni and Al. These specific edges were chosen for imaging by adapting a strategy [15], whereby the imaging conditions were optimized for both better signal-to-noise ratio (SNR) and contrast-to-noise ratio. The brighter regions in these images are richer in their respective elements. EFTEM mapping using ionization edges that normally lie in the low-loss-region (30-90 eV) were mostly avoided due to excessive overlapping of the edges (which would require complex de-convolution methods). However, in the case of Al, despite being in the low loss region, the Al L-edge (73eV) was still chosen because it had a higher intensity compared to the Al-K edge (1560 eV), which was too far out in the electron energy loss spectroscopy (EELs) spectrum.

The EFTEM images obtained using the different elements were subjected to rigorous stereological measurements. In the semi-automated mode, the individual precipitates were manually traced and quantified with the help of FoveaPro© software. In the fully automated mode, various image segmentation techniques (in-house developed) were utilized to effectively delineate the precipitates from the matrix. Once the precipitate/matrix boundaries were identified, the sizes of the precipitates were measured using different methods, as discussed in section 3.2.

3.2 Manual and automated techniques

It is important to note that imaging with different elemental edges can also highlight artifacts associated with imaging. An example of such a case is shown in Figure 3 where a single particle that is visible in the Ti-L EFTEM image shows up as two separate particles in the Cr-L EFTEM image of the same location.

A total of 51 particles from the eight locations were processed using the manual trace and automated methods. An example of the automated area method is shown in Figure 4. Figure 4(a) shows the original image of the precipitate using the Cr-L element edge, while Figure 4(b) shows the bounding box and thresheld image using the procedure shown in Figure 4(c) and 4(d). As the bounding rectangle begins, it encompasses the entire image region (since all intensity values fall within the range). However, as the minimum threshold parameter increases, the bounding box size decreases; the rate changes rapidly at the precipitate boundary. This is indicated on the plots in Figures 4(c) and 4(d) by the change in slope at the minimum threshold parameter of 94. Figure 4(d) is a magnified plot of the intensity to highlight the slope change. Once the precipitate boundary is crossed, independent regions develop within the image. This technique then treats the new unconnected regions as separate particles, which reduces the pixel counts within the main particle. For simplicity, Figures 4(c) and 4(d) only plot out the number of pixels for the main precipitate, so at large minimum threshold parameters, the curve declines sharply as smaller particles are formed within the image. Results for the method comparisons are shown in Table 3, which includes the values obtained using the manual boundary trace method. The average equivalent diameter values for the automated methods were within 7.6 % of the values obtained using the manual method. In fact, the average equivalent diameter

determined using the automated area method compared within 1.4% with the value determined using the manual method, with a very similar standard deviation of 6.953 (compared to 6.890).

The automated area method was used to analyze one particle from each of the 8 locations imaged using the 5 elements. The resulting intensity curves are shown in Figure 5. The curves for Cr-L, Ni-L, and Ti-L were less sensitive to the changes in the intensity values for the region of interest. This is reflected by the reduced slope of the curve as the minimum threshold parameter increases past the precipitate boundary pixel value in the image. The intensities of the Cr-L images were inverted to compare with the other element images. The choice of these element edges provided insight into the impact of choosing elements that were segregated to the matrix (Cr) or to the precipitate (Ti, Ni). Based on these results, the Cr-L, Ni-L, and Ti-L edge EFTEM elements were chosen for the final evaluation and comparison.

The manual trace method was used for a final evaluation of the particles. The method was found to provide similar results to the automated area method and was easier to apply without cropping the precipitates from the images. Each of the Cr-L EFTEM element edge images were evaluated for all viable precipitates (total of 157) from 8 different locations. The resulting average equivalent diameter was 33.567 nm, with a standard deviation of 7.504 nm. A similar evaluation using the Ti element edge images provided an average equivalent diameter of 33.351 nm with a standard deviation of 7.710 nm for 163 precipitates. For the Ni EFTEM element edge image evaluation, the average equivalent diameter was 33.924 nm with a standard deviation of 8.860 for 148 precipitates. The three techniques provided equivalent diameter values within +/- 1.8%. Using the following equation for the estimated error:

$$\text{Standard error} = \sigma / \sqrt{N} \qquad (3)$$

where σ is the standard deviation, and N is the sample number of precipitates, the estimated standard errors using the three elements are between 0.599 and 0.731 nm. Cr-L was chosen as the preferred element edge because the Cr-L images provided clearer boundaries where particles overlapped, and the results were comparable with the diameters determined using the Ti-L element images.

3.3 Region Growing Technique

The approach was tested using the same 51 γ' precipitates from the Cr-L EFTEM images that were used for the automated area evaluation method. For the following analysis, the region growing technique used a density-based weighting function with two independent parameters [24]. As can be observed in Figure 6, the measured precipitate size increased with increasing threshold parameter for the 16-bit EFTEM images. However, in the absence of a proper stopping criterion for the region growing algorithm, the choice of threshold parameter can greatly affect the measured size of the precipitate. Figure 7(a) shows the mean intensity values and the intensity difference relating to the automated stopping criterion for the region growing technique. Recalling that the automated stopping criterion compares the mean intensity from inside the region to that outside the region, it is evident that for small threshold parameters, the intensity of the area outside the region is approximately equivalent to the intensity of the area inside the region, i.e., the majority of the pixels within both areas lie within the precipitate.

However, as the region grew towards the diffuse precipitate interface, the intensities in both areas decreased. The difference between the mean intensities for these two areas is also shown in Figure 7(a). We define the optimum segmentation of the precipitate as the threshold parameter that gives the maximum intensity difference between these two areas. The routine quantitatively identified the boundary of the precipitate based on the intensity value gradient across the interface, as shown in Figure 7(b) where the red boundary line has been overlaid onto the original image. The resulting average equivalent diameter for the precipitates was 35.834 nm with a 2.99% difference when compared with the result obtained using the manual trace method.

The difference between the two methods could be minimized by altering parameters related to the neighborhood size and weighting factors or by defining a stopping criterion that more closely matches manual segmentation. However, for this study the values chosen provided a growth shape compliant with the spherical nature of the precipitate, and also allowed routine completion within an acceptable time constraint. For the purposes of measuring the precipitate diameter and area fraction, the parameters used for the region growing technique were acceptable. Further work analyzes the sensitivity of the precipitate diameter and area fraction to the region growing parameters [24] and how to reduce the differences between the region growing routine and the manual trace method. One advantage over previously discussed automated methods is that once the optimum parameters are determined, the region growing algorithm requires no user intervention. At present, the automated area method still requires the user to select the optimum minimum threshold parameter based on the plots.

4.0 Conclusions

1. Although the Cr EFTEM images contained more contrast information, especially in the case of precipitates that overlapped on the image, the measured precipitate areas and diameters were similar to the values obtained from the Ni and Ti EFTEM images (within 1.8% difference). As a result, the Cr electron-energy loss edge provided the best contrast between the γ and γ' phases in the EFTEM images, followed closely by Ti and Ni. W, Al and Co did not provide the same quality of data in the corresponding EFTEM images.

2. The EFTEM images acquired using electron-energy loss edges corresponding to the elements that partition to the γ matrix exhibited higher contrast for small precipitates as compared with the images acquired using the edges for elements partitioning to the γ' phase. This was easily observed for the Cr EFTEM images where small precipitates (less than 5 nm) were clearly visible at locations where they were not as visible using Ti and Ni energy loss edges.

3. The automated approaches worked well when run with direct user observation of the bounding regions. Resulting changes in the number of pixels within the intensity range versus the minimum intensity values provides a possible mathematical tool for determining precipitate size directly from intensity data. The automated procedures provided results within 8% of each other, and compared favorably to the manual trace process typically used.

4. The region growing technique provides a reproducible, automated approach for measuring precipitate area diameters and identifying interfaces with diffuse intensity gradients. Future work will examine optimizing region growing parameters to more closely match precipitate statistics corresponding to those from manual segmentation.

5. Acknowledgements

This research was supported by the Air Force Research Laboratory (AFRL/RXLM) under the Institute for Science and Engineering Simulation, Contract FA8650-08-C-5226. In addition, material preparation support was provided by Mr. Kevin Shiveley and the Materials Characterization Facility at AFRL/RX.

6. References

1. Reed R.C, The superalloy, fundamentals and applications. Cambridge University Press; (2006) pp. 236.
2. Telesman, J., et al., In: Green, K.A., et al., editors. Superalloys 2004. Warrendale, PA: TMS Publications; (2004)pp. 215.
3. Stoloff, N.S., In: Sims, C.T., et al., editors. Superalloys II. New York: John Wiley: (1987) pp.61.
4. Sondhi, S.K., et al., Acta Materialia 52 (2000) pp. 1761.
5. Fahrmann, M., et al., Mater. Sci Eng, A271 (1999) pp.122
6. Sarosi, P.M., et al. , Scripta Mater 57 (2007) pp.767.
7. Wen, Y.H., et al., Acta Materialia 54 (2006) pp.2087.
8. Hwang, J.Y., et al., Metallurgical and Mat Trans A, Vol 40A (2009) pp.24.
9. Wlodek, S.T., et al.,editors, Superalloys 1996, Warrendale PA: TMS; (1996) pp. 129.
10. Tiley, J., et al., Acta Materialia 57 (2009) pp. 2538-2549.
11. Hwang, J.Y., et al., Scripta Materialia 61 (2009) pp. 92-95.
12. Kriege, O.H., Baris, J.M., Transactions of the ASM, Vol 62 (1969) pp.195.
13. Gayda, J., and Gabb, T., Glenn Research Center, National Air and Space Administration, (2009) unpublished research.
14. Viswanathan, G.B., et al.,Acta Materialia, 53 (2005) pp.3041.
15. Sarosi, P.M., et al., Ultramicroscopy, 103 (2005), pp. 83.
16. Unocic, R.R., et al., Adv. Mater. Proc. 163 (2005), pp. 50.
17. Collins, P.C., et al., Materials Science and Eng A 508 (2009) pp.174-182.
18. Tiley, J., et al., Searles Mat Science and Eng A 372 (2004) pp. 191-198.
19. Littles, Jr., J.W., et al., In: Materials damage prognosis. Warrendale, PA: TMS Publications (2005) pp.23.
20. Fovea Pro® Software, Reindeer Graphics, 2003.
21. Adobe Photoshop ® CS2 Software, Adobe Systems Inc., 2005.
22. Labview™ Sofware, National Instruments, 2005.
23. NI Vision, Labview™ Software manual, 372916F-01, National Instruments (2007).
24. Tschopp, M.A., et al., Materials Science and Technology (2009), submitted for publication.
25. Srinivasan, R., et al., Phys. Rev. Lett., 102(8), (2009) 086101.

Table Captions:

Table 1: Composition of Rene88DT water quenched sample

Table 2: Energy Filtered Transmission Electron Microscopy ionization edges

Table 3: Results for different processing methods used in determining the equivalent diameter of precipitates

Figure Captions:

Figure 1: Chemical segregation between the γ' precipitates and matrix γ in RENE88DT water quenched samples as determined from atom probe tomography [24]. The interface boundary is at the 4.5 nm distance value.

Figure 2: EFTEM image particles for Al, Ti, Cr, and Ni element edges. Images are from location 1.

Figure 3: EFTEM images of location 2 using Ti and Cr element edges. Note the added contrast detail for the Cr edge image for the overlapped middle particles that appear as one particle in the Ti image.

Figure 4: a) original image, b) bounding box of particle, c) plot of pixel count for minimum intensity values, d) the change in the slope at intensity parameter equals 94 provides the boundary.

Figure 5: Particle pixel count plots for different EFTEM element images, for a particle in location 1.

Figure 6: Pixel number plot versus the intensity values for the Region Growing Routine, with the neighborhood particle value of 5. The data represents particle 6 of location 8 imaged using the Cr element edge.

Figure 7: Data for particle 6 of location 8 imaged using the Cr element edge.
a) Pixel number plot versus the intensity values for the Region Growing Routine, with the weight function comparison factor equal to 9, b) overlay of the interface boundary (in red) on the original image.

Figures and Tables

Table 1

	Al	Ti	Cr	Co	Ni	Nb	Mo	W	C	B
Average (wt%)	2.09	3.92	16.24	13.27	56.53	0.76	4.08	3.92	0.049	<0.03

Table 2

Element	Ionization Edge (eV)	Slit Width (eV)	Post Edge Position 1 (eV)	Pre Edge Position 1 (eV)	Pre Edge Position 2 (eV)
Ti-L	456	30	471	441	426
Cr-L	575	30	590	560	530
Co-L	779	30	794	764	749
Ni-L	855	30	870	840	825
Al-L	73	10	78	68	63

Table 3

Method	Equivalent Diameter (nm)	Error (difference with manual)
Manual Trace of Area	36.939	
Diagonal of Bounding Box	37.833	2.42%
Maximum Feret	39.75	7.61%
Area Intensity	37.437	1.34%
Region Growing Routine	35.834	2.99%

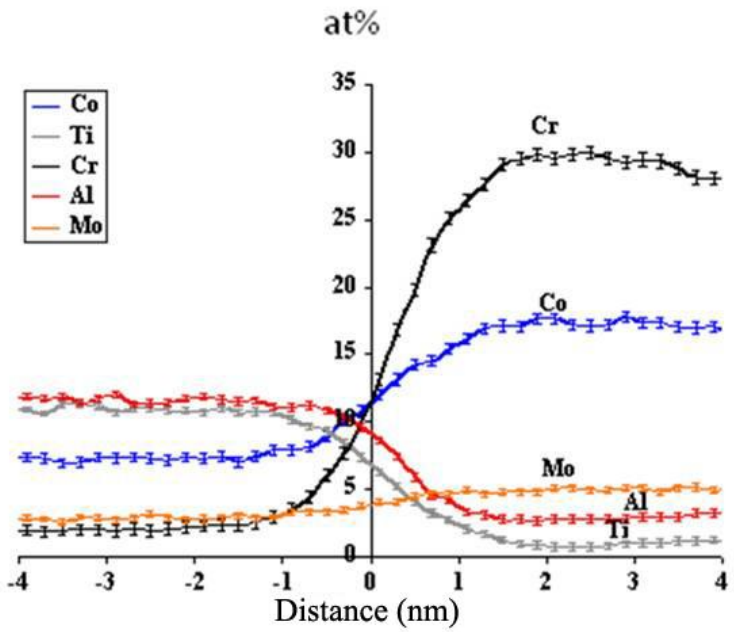

Figure 1

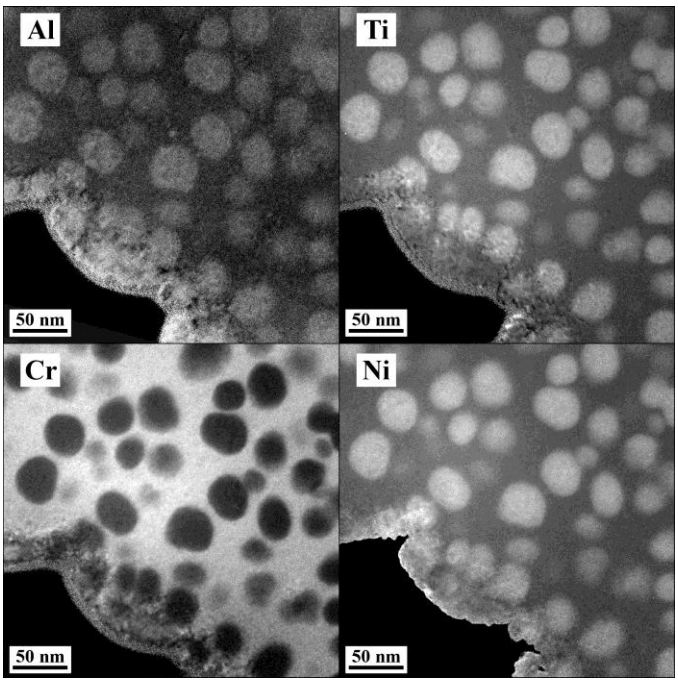

Figure 2

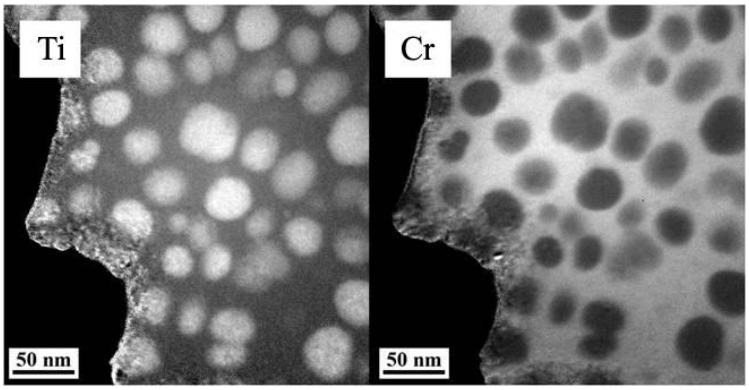

Figure 3

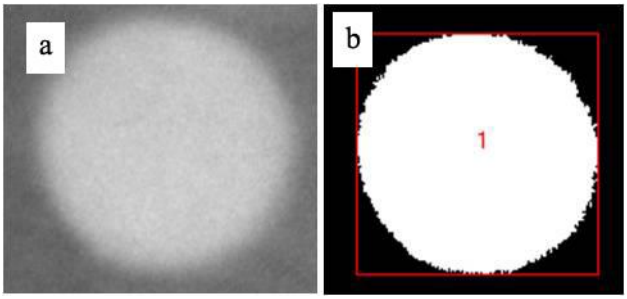

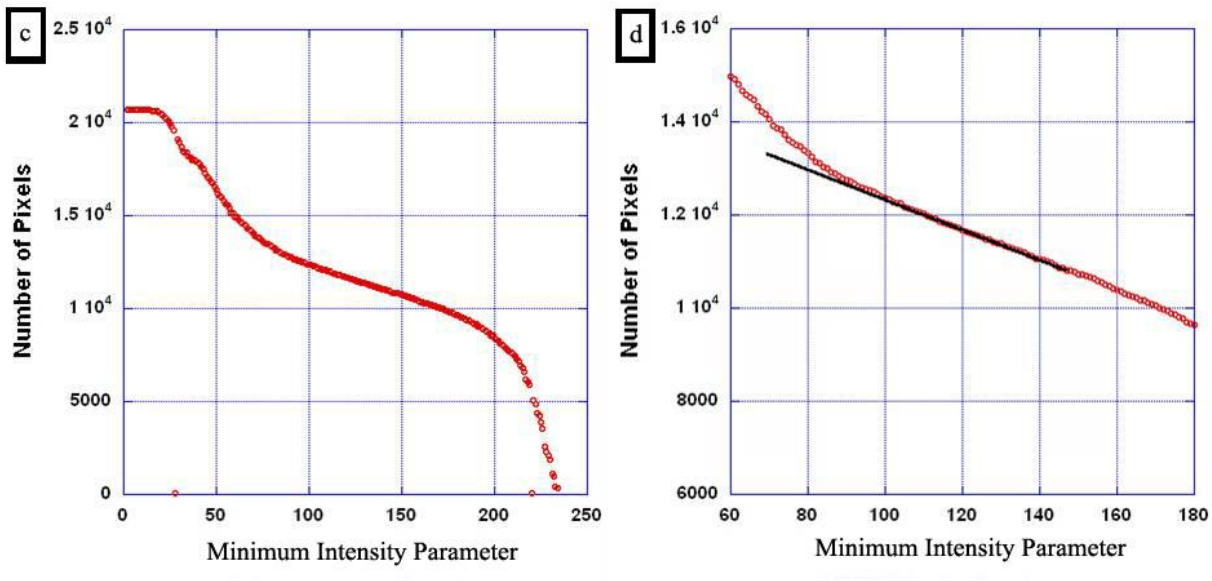

Figure 4

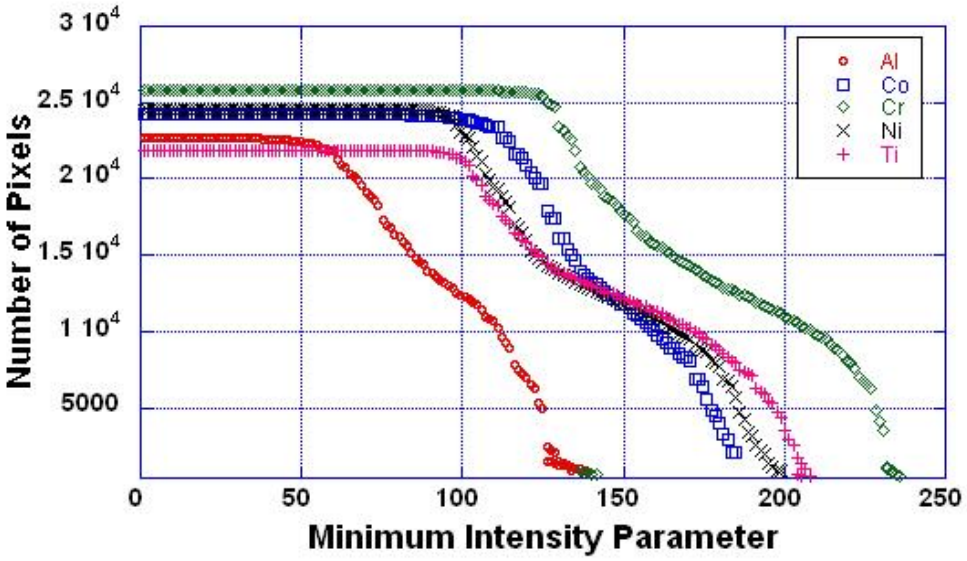

Figure 5

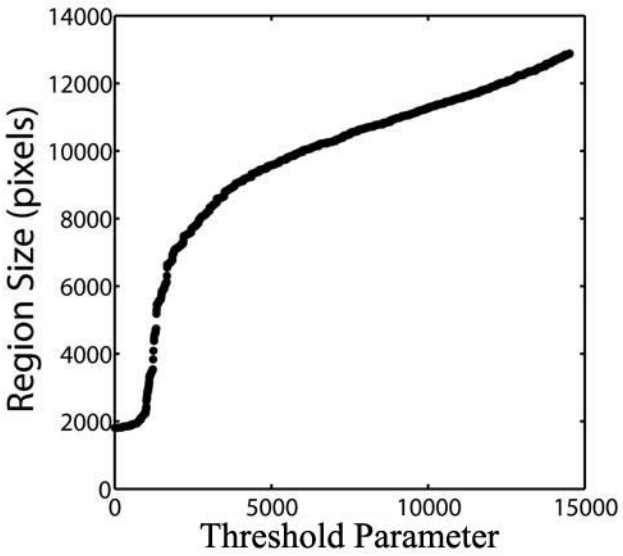

Figure 6

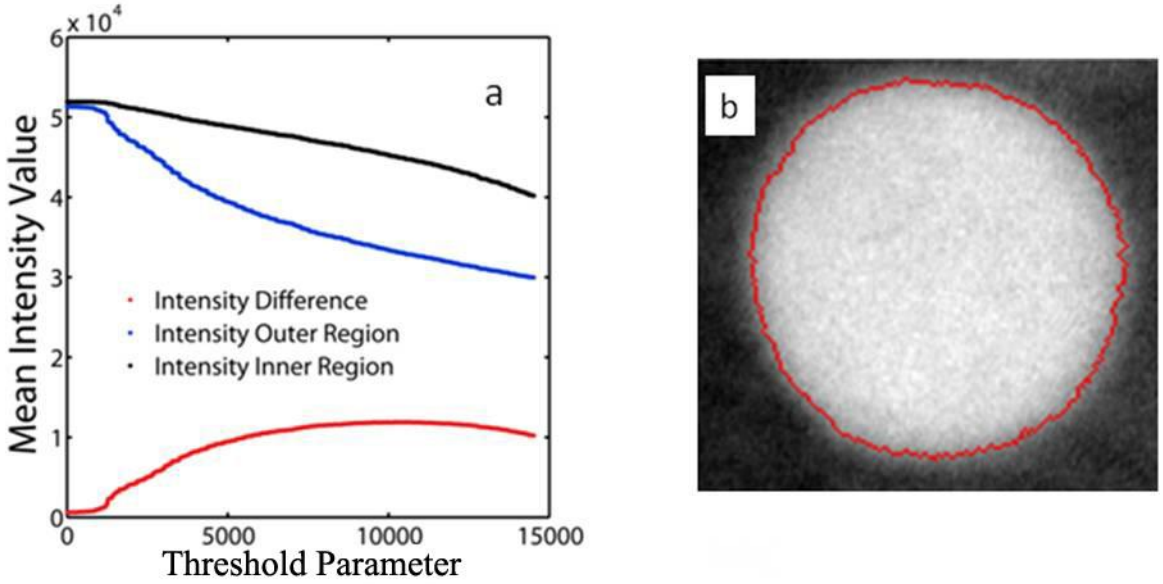
x 10^4
6
5
4
3
2
1
0
a
Mean Intensity Value
Intensity Difference
Intensity Outer Region
Intensity Inner Region
0
5000
10000
15000
Threshold Parameter
b

Figure 7